Journal of Materials Chemistry A

Highly Stretchable, Self-Adhesive, Biocompatible, Conductive Hydrogels as Fully Polymeric Strain Sensors

Journal:	*Journal of Materials Chemistry A*
Manuscript ID	TA-ART-07-2020-007390.R1
Article Type:	Paper
Date Submitted by the Author:	28-Aug-2020
Complete List of Authors:	Zhang, Dong; University of Akron Tang, Yijing; University of Akron, Department of Chemical, Biomolecular, and Corrosion Engineering Zhang, Yanxian; University of Akron, Department of Chemical, Biomolecular, and Corrosion Engineering Yang, Fengyu; University of Akron, Department of Chemical, Biomolecular, and Corrosion Engineering Liu, Yonglan; University of Akron, Chemical and Biomolecular Engineering Wang, Xiaoyu; Zhejiang University of Technology, College of Materials Science& Engineering Yang, Jintao; Zhejiang University of Technology, Gong, Xiong; University of Akron, Polymer Eng Zheng, Jie; University of Akron, Department of Chemical, Biomolecular, and Corrosion Engineering

Highly Stretchable, Self-Adhesive, Biocompatible, Conductive Hydrogels as Fully Polymeric Strain Sensors

Dong Zhang[1], Yijing Tang[1], Yanxian Zhang[1], Fengyu Yang[1], Yonglan Liu[1], Xiaoyu Wang[2], Jintao Yang[2], Xiong Gong[3], and Jie Zheng[1, 3]*

[1] Department of Chemical, Biomolecular, and Corrosion Engineering
The University of Akron, Akron, Ohio 44325, USA

[2] College of Materials Science& Engineering
Zhejiang University of Technology, Hangzhou, 310014, P. R. China

[3] Department of Polymer Engineering
The University of Akron, Akron, OH 44325, USA

*Corresponding Author: zhengj@uakron.edu

Abstract

Development of highly stretchable and sensitive soft strain sensors is of great importance for broad applications in artificial intelligence, wearable devices, and soft robotics, but it proved to be profound challenges to integrate the two seemly opposite properties of high stretchability and sensitivity into a single material. Herein, we designed and synthesized a new fully polymeric conductive hydrogel with interpenetrating polymer network (IPN) structure made of conductive PEDOT: PSS polymers and zwitterionic poly(HEAA-*co*-SBAA) polymers to achieve a combination of highly mechanical, biocompatible, and sensing properties. The presence of hydrogen bonding, electrostatic interactions, and IPN structures enabled poly(HEAA-*co*-SBAA)/PEDOT: PSS hydrogels to achieve ultra-high stretchability of 4000-5000%, tensile strength of ~0.5 MPa, rapid mechanical recovery of 70%-80% within 5 min, fast self-healing in 3 min, and strong surface adhesion of ~1700 $J \cdot cm^{-2}$ on different hard and soft substrates. Moreover, the integration of zwitterionic polySBAA and conductive PEDOT: PSS allowed to facilitate charge transfer via optimal conductive pathways. Due to its unique combination of superior stretchable, self-adhesive, and conductive properties, the hydrogels were further designed into strain sensors with high sensing stability and robustness for rapidly and accurately detecting subtle strain- and pressure-induced deformation and human motions. Moreover, an in-house mechanosensing platform provides a new tool to real-time explore the changes and relationship between network structure, tensile stress, and electronic resistance. This new fully polymeric hydrogel strain sensor, without any conductive fillers, holds great promise for broad human-machine interface applications.

Keywords: Conductive hydrogels, Polymer, Strain sensors, stretchability, PEDOT:PSS, IPN

Introduction

Rapid advances of soft-smart sensors have received great interests for their broad applications in wearable devices, smart robotics, and artificial intelligence. Different from elastomer-based sensors, developing hydrogel-based strain sensors are highly desirable but more challenging for electronic skins, health monitors, and human-machine interfaces[1-11], due to the presence of high content water (>50-90%) in polymer networks. High content water in hydrogels, on one hand, offers unique and excellent biomimetic and biocompatible properties; on the other hand, compromises the rapid and efficient conversion of small-scale pressure-induced motion/deformation to measurable electronic signals. To develop highly sensitive and robust hydrogel-based strain sensors, several major roadblocks need to be addressed, i.e., high stretchability and conductivity are required and often coupled to withstand large deformation and maximize the conversion from mechanical deformation to electronic signals. Strong surface adhesion of conductive hydrogels on substrates is also a critical factor to avoid the interfacial debonding of adhered hydrogels and subsequent loss of functionality (i.e. sensitivity, reliability, repeatability). Additionally, hydrogel strain sensors are nontoxic and biocompatible.

In light of these challenges, two common design strategies are often used for fabricating ultrasensitive hydrogel strain sensors. The first strategy is to fabricate nanocomposite hydrogels by introducing highly conductive nanomaterials, including carbon nanomaterials [12], noble metal nanoparticles [13], polyelectrolytes [14, 15], and ionic liquids [16], into polymer matrix. For instance, polyvinyl alcohol (PVA)/MXene [17], PVA/single-wall carbon nanotube (SWCNT) [18], poly acrylic acid (polyAAc)/nano barium ferrite ($BaFe_{12}O_{19}$) [19], and polyacrylamide (polyAAm)/salt hydrogels [20, 21] have been fabricated into soft strain sensors for real-time detection of different-scale human motions (finger touching, arm bending/twisting, wrist pulse, and blood pressure). The superior conductivity from 2D nanomaterials or high concentrations of inorganic salts enables nanocomposite hydrogel sensors to achieve high gauge sensitivity of 2-100, but inevitable heterogeneous distribution of nanocomposites and salt precipitation often causes structural incompatibility between rigid nanocomposites/salts and flexible polymer network to compromise their stretchability, thus greatly affecting their stretching-induced sensing ability, repeatability, and robustness.

Another strategy to improve stretchability and conductivity is to directly fabricate conductive polymers (e.g. PEDOT: PSS, polyaniline, and polypyrrole) into hydrogel strain sensors, simply because of their intrinsic, conductive ionic groups[22-32]. Moreover, the intrinsic soft-conjugated chains in conductive polymers offer great structural flexibility and compatibility to accommodate with other polymers in the same hydrogel systems for empowering their high stretchability. Using this design strategy, fully-polymeric hydrogel sensors, such as poly(AAm-*co*-hydroxyethyl methacrylate (HEMA))/polyaniline (PANI) [22], PSS-UPyMA/PANI [33], and poly(N-isopropylacrylamide)/PANI [34], have been developed for tracking normal human movements with high sensing ability (gauge factor is up to ~11). However, challenges still remain. Such conductive hydrogel strain sensors suffer from weak mechanical strength (tens of kilopascals) and poor fatigue resistance to repeatable stretching/compression, presumably due to lack of strong network interactions and efficient energy dissipation modes [35-38]. While the co-polymerization of conducting and non-conducting polymers could enhance mechanical properties to some extents, the interpenetrating network structures also introduce steric barriers to decrease electronic

conductivity. Therefore, it remains a great challenge to develop fully polymeric hydrogel sensors without adding any conductive nanofillers but still possessing high stretchability and sensitivity simultaneously. Additionally, achieving strong adhesion property of hydrogels requires two main factors: high mechanical properties of bulk hydrogel itself and strong interfacial bonding between hydrogel and substrate. Design of tough hydrogels (e.g. double-network hydrogels, IPN hydrogels, and nanocomposite hydrogels) with integrating surface adhesion motifs is often used to fulfil the above criteria. Use of stealth or inert materials allows to prevent biomacromolecules adhesion while still preserving the functions of the hydrogels adhered on the substrates.

Here, we designed and fabricated fully polymeric conductive hydrogels by interpenetrating PEDOT: PSS conductive polymers into zwitterionic poly(HEAA-*co*-SBAA) network to achieve a combination of highly mechanical (stretchable, self-adhesive, and self-healable) and functional (strain sensing and biocompatible) properties (Figure 1). From a mechanical viewpoint, by integrating multiple physical crosslinkings by hydrogen bonding, electrostatic interactions, and chain entanglement within and between interpenetrating polymer network (IPN), the resultant poly(HEAA-*co*-SBAA)/PEDOT: PSS hydrogels achieved ultra-high stretchability of 4000-5000%, tensile strength of ~0.5 MPa, fast stiffness/toughness recovery of 70%/80% after 5-min resting, and rapid self-healing after 3 min resting at room temperature without any external stimuli. From a conductivity viewpoint, the integration of highly balanced charges of zwitterionic network with highly conductive PEDOT: PSS polymers facilitated charge transfer via optimal conductive pathways. The hydrogels also demonstrated their high antifouling property to resist the surface adhesion of both bacteria and cells. So, a unique combination of superior mechanical, self-adhesive, biocompatible, and conductive properties endows the poly(HEAA-*co*-SBAA)/PEDOT: PSS hydrogels to be designed into a dual-sensitive strain sensor, which provides highly sensitive, reliable, and precise monitoring of full-range human activities.

Different from traditional strain sensors that performed variable one-way positive gauge factor, the mechanism for reconstruction and optimization of conductive PEDOT: PSS combining polyzwitterionic network was proposed to describe abnormal resistance reduction at lower stretching rates and verified by a real-time sensing process. This work demonstrates a delicate design strategy for a fully polymeric hydrogel strain sensor to simultaneously realize high mechanical and sensing ability, comparable to or even better than those hydrogel sensors with addition of conductive nanocomposites or salts.

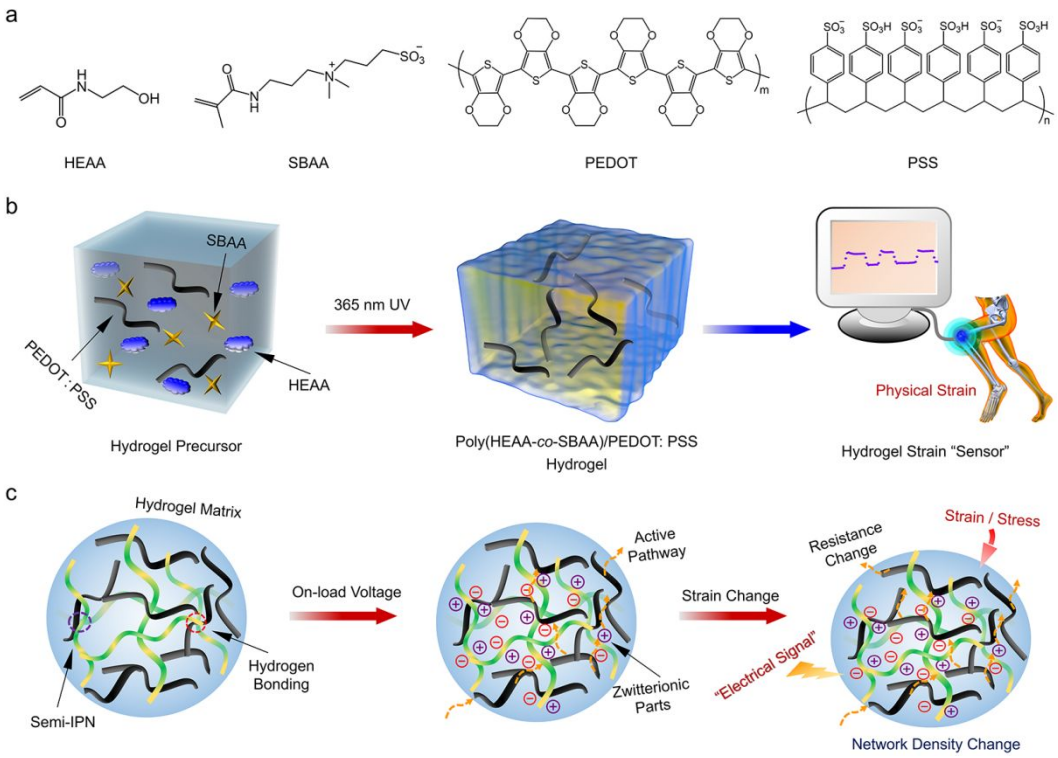

Figure 1. A design strategy for a fully polymeric hydrogel strain sensor. (a) Chemical structure of individual components of HEAA, SBAA, PEDOT, and PSS for preparing poly(HEAA-*co*-SBAA)/PEDOT: PSS hydrogel as a strain sensor. (b) One-pot, two-step fabrication process for poly(HEAA-*co*-SBAA)/PEDOT:PSS hydrogel sensors. (c) Sensing mechanism of the hydrogel strain sensor. The IPN structure of this conductive hydrogel is physically crosslinked by hydrogen bonds between hydrophilic polyHEAA and electrostatic interactions between zwitterionic polySBAA and conductive EDOT: PSS polymers. Zwitterionic polySBAA in poly(HEAA-*co*-SBAA) offers a large amount of charge transfer sites within and between PEDOT: PSS macromolecular chains. As deformation is applied to the hydrogel, optimal conductive pathways are constructed to facilitate charge transfer and thus amplify electric signals.

Results and Discussions

Fabrication and mechanical characterization of poly(HEAA-*co*-SBAA)/PEDOT: PSS hydrogels

Figure 1b shows the one-pot, two-step fabrication procedure for a fully physical conductive hydrogel consisting of a poly(HEAA-*co*-SBAA) network cross-linked by hydrogen bonds and semi-interpenetrated with conductive PEDOT: PSS polymers. Briefly, a mixture of HEAA monomers, SBAA monomers, and UV initiator was dissolved in pre-whipped PEDOT: PSS aqueous solution, followed by the photo-polymerization to form poly(HEAA-*co*-SBAA) network by UV light (8 W). During the synthesis process, PEDOT: PSS polymers were uniformly interpenetrated into polyzwitterionic network, but without involving any chemical crosslinker. As an anisotropic hydrogel, we considered three major structural designs to work synergistically for achieving highly conductive and mechanical properties: (i) no any chemical crosslinker was introduced to form poly(HEAA-*co*-SBAA) network in order to prevent the formation of non-conductive medium among networks; (ii) copolymerization of zwitterionic polySBAA with polyHEAA allowed to provide

abundant ionic sites for create more conductive pathways for charge transfer; (iii) literature review showed that zwitterionic-based hydrogels always had weak mechanical properties. In this design, a small addition of zwitterionic monomers (0.4 g) can prominently improve the mechanical strength of poly(HEAA-*co*-SBAA)/PEDOT: PSS hydrogels, presumably due to IPN structures and the improved inter-network interactions. FT-IR spectra in Figure S1 shows the side-by-side comparison for chemical structure variation between polyHEAA and conductive poly(HEAA-*co*-SBAA)/PEDOT: PSS hydrogels. For poly(HEAA-*co*-SBAA)/PEDOT: PSS hydrogel, distinct characteristic peaks located at 1132 cm^{-1}, 990 cm^{-1}, and 842 cm^{-1} were observed, corresponding to stretching vibration of para di-substituted aromatic derivative and bending vibration of -S=O from doped polymers (PEDOT: PSS) and sulfonate residues [39, 40]. Both hydrogels shared the common peaks at ~1680 cm^{-1} and 1450 cm^{-1}, corresponding to the stretching vibration of -NH-CO- and -OH groups[41]. Furthermore, 2D-FTIR synchronous spectra in Figure S2 showed that as temperature increased from 25 ^{o}C to 50 ^{o}C, concentrated area at ~1040 cm^{-1} corresponding to the associated SO_3^{2-} groups gradually transformed to the disassociated SO_3^{2-} state at 1030 cm^{-1}, while the characteristic area of –C=O group at ~1710 cm^{-1} gradually spread to ~1680 cm^{-1} (left panel). Similar trend was also observed in 2D asynchronous spectra (right panel). These results suggest that zwitterionic groups become disassociated state as increase of temperature, leading to the reduction in electrostatic interactions. In addition, as is shown in Table S1, both microgels and tiny fragments (bulk gel) exhibited nearly uncharged state, as the zeta potential located at 1.08±0.3 mV and -0.66±0.5 mV. This zeta potential result demonstrates that while hydrogen bonding and electrostatic interactions are existed in the hydrogels, the actual potential is approaching neutral without the interference of acidic solvents inside.

Upon obtaining conductive poly(HEAA-*co*-SBAA)/PEDOT: PSS hydrogels, we first systematically measured their mechanical performances using tensile, load-unloading, and self-healing tests. At a first glance, a typical thin gel cylinder enabled to lift 100 g/200 g weights without breaking, presenting strong mechanical performance (Figure 2a). When applying a typical dumbbell-shaped hydrogel to a tensile test, the hydrogel can be stretched up to 5000%, a maximal stretching limit of the Instron 3345, without breaking (Figure 2b). Such ultra-stretchability of poly(HEAA-*co*-SBAA)/PEDOT: PSS hydrogels have far exceeded most of hydrogel systems. Of technical note that many so-called ultra-stretching hydrogels with high stretchability of >3000% were often used gel cylinders rather than dumbbell-type samples for tensile test [42, 43].

To explore the effect of zwitterionic polymer on mechanical improvement for poly(HEAA-*co*-SBAA)/PEDOT: PSS hydrogels, we prepared a series of conductive hydrogels by varying the SBAA contents of 0~0.8 g and quantified their tensile properties of the gels in response to SBAA contents. In Figure 2c-d, as the SBAA contents slightly increased from 0 g to 0.2 g, poly(HEAA-*co*-SBAA)/PEDOT: PSS hydrogels increased tensile stress from 0.36 MPa to 0.49 MPa and corresponding tensile strain from ~2230% to ~4104%, but corresponding elastic modulus sharply decreased from 0.18 MPa to 0.05 MPa. Further increase of SBAA contents led to the monomeric drop of tensile stress/elastic modulus to 0.34 MPa/0.024 MPa, 0.27 MPa/0.013 MPa and 0.07 MPa/0.015 MPa at the SBAA contents of 0.4 g, 0.6 g, and 0.8 g, respectively. But, poly(HEAA-*co*-SBAA)/PEDOT: PSS hydrogels became very elastic and soft so it can be stretched up to 9700 % at 0.8 g SBAA. The SBAA-dependent mechanical

properties suggest that SBAA may act as crosslinkers at an optimal contents to maximize electrostatic interactions between zwitterionic SBAA and highly acidic PEDOT: PSS while reducing over-crosslinking effects by SBAA. In addition, as is shown in Figure S3, poly(HEAA-*co*-SBAA) hydrogel without PEDOT:PSS exhibited ~0.17 MPa of tensile stress and ~3400% of stretchability, which were much lower than ~0.34 MPa of tensile stress and ~5000% of stretchability of poly(HEAA-*co*-SBAA)/PEDOT: PSS hydrogels. This indicates that the introduction of PEDOT: PSS into zwitterionic poly(HEAA-*co*-SBAA) hydrogel enables to largely improve its mechanical properties via enhanced electrostatic interactions between PEDOT: PSS and zwitterionic groups.

To better understand both energy dissipation and mechanical recovery of poly(HEAA-*co*-SBAA)/PEDOT: PSS hydrogels, poly(HEAA-*co*-SBAA)/PEDOT: PSS hydrogel prepared at 0.4 g SBAA was selected and tested by both cyclic and successive loading-unloading tests (Figure S4-S5). As a typical cyclic loading-unloading test in Figure 2e, in the first loading-unloading cycle, poly(HEAA-*co*-SBAA)/PEDOT: PSS hydrogel displayed a relative large hysteresis loop and high energy dissipation of 0.12 $MJ \cdot m^{-3}$ at a large strain of 900%. In the immediate second loading-unloading cycle without resting, the hysteresis loop was reduced to ~70% of original one, and this loop remained almost unchanged in the following third or fourth cycles. Quantitatively, Figure 2f showed the toughness/stiffness recovery of ~68%/82%, 65%/79%, and 64%/80% for the second, third, and fourth loading-unloading cycles, respectively. These results indicate that multiple physical interactions between networks can be rapidly and reversibly formed and broken even at large deformation strain with the less scarification of mechanical properties, which offers a potential application for hydrogel strain sensors. We further investigated the fatigue resistance of poly(HEAA-co-SBAA)/PEDOT:PSS hydrogels at a larger strain of 1000% using 4 cyclic loading-unloading test and another strain of 1200% using 2 cyclic loading-unloading test, respectively. As a result, both toughness/stiffness recoveries were reduced as an increase of strains, as evidenced by ~36%/~45% at a strain of 1000% and 0%/~30% at a strain of 1200%. (Figure S6). Thus, from a practical viewpoint, it is necessary to balance high fatigue resistance and sustainable sensitivity/duration of poly(HEAA-co-SBAA)/PEDOT:PSS hydrogel sensors to achieve their best sensing performance at an optimal strain of 900%.

Furthermore, a large amount of physical hydrogen bonds and electrostatic interactions could empower poly(HEAA-*co*-SBAA)/PEDOT: PSS hydrogels to have self-healing property. Figure 2g and 2h illustrated the rapid self-healing of the hydrogels at both macroscopic and microscopic scales. Specifically, after two cut hydrogel samples were simply placed together without applying external force and stimuli for 3 min, the two gels were self-healed into a single gel, which can be directly stretched up to ~210%. Optical microscopic images in Figure 2h further showed that after the gel was cut by a knife, the wound of the gel was quickly closed to form a smooth surface at room temperature within 10 min. Furthermore, we conducted the tensile tests for the self-healed poly(HEAA-*co*-SBAA)/PEDOT: PSS hydrogels after 3, 5, 10 min self-healing. It can be seen in Figure S7 that the after 3 min self-healing, self-healed poly(HEAA-*co*-SBAA)/PEDOT: PSS hydrogel can recover its tensile strain/stress of ~40%/25% relative to those of original intact hydrogel, and further increase of self-healing time to 5 and 10 min appeared not improve the mechanical recovery properties. This may imply that self-healing at the interface connected to the two cut hydrogel pieces is a control factor for mechanical recovery.

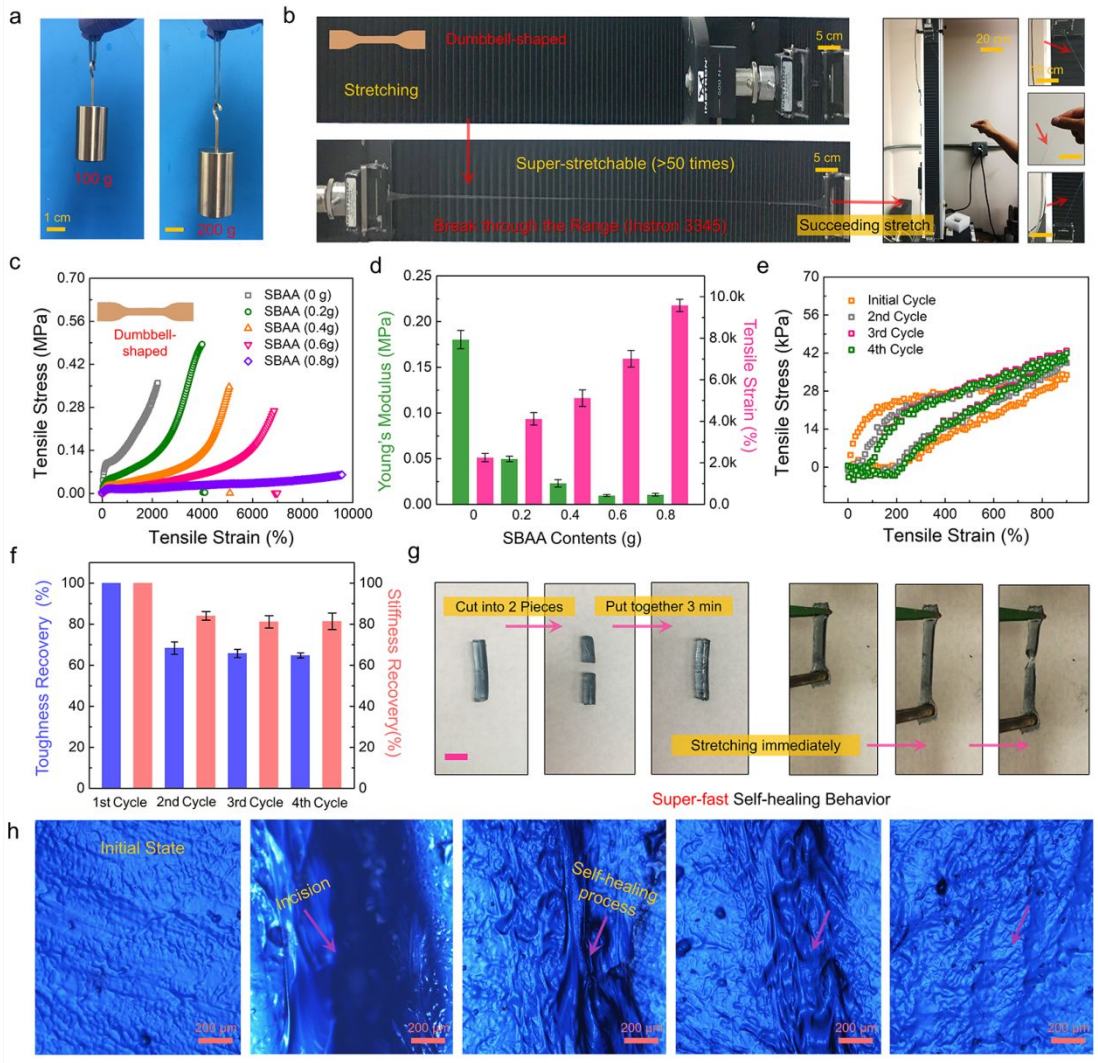

Figure 2. Mechanical, self-recovery, and self-healing properties of poly(HEAA-*co*-SBAA)/PEDOT: PSS hydrogels. (a) A thin hydrogel cylinder to lift 100 g and 200 g weights; (b) Ultra-stretchability of a dumbbell-shaped hydrogel (thickness: 1 mm) up to ~5000%; Zwitterionic SBAA contents effects (0~0.8 g) on (c) tensile stress-tensile strain and (d) elastic module-tensile strain of the hydrogels. (e) Cyclic loading-unloading curves and (f) the corresponding toughness/ stiffness recovery of the hydrogels at a strain of 900%. (g) Visualization of a fast self-healing process of the hydrogel within 3 min. (h) Optical micrographs of the self-healing of hydrogel incision within 10 min. at room temperature.

Strong surface adhesion of poly(HEAA-*co*-SBAA)/PEDOT: PSS hydrogels on nonporous solids

Apart from high mechanical properties, hydrogel-based sensors also require high surface adhesion to realizing their sensing ability. However, not all tough hydrogels are surface adhesive to solid surfaces with weak interfacial toughness of several hundreds of $J \cdot cm^{-2}$, or vice versa, because surface adhesion requires additional surface-hydrogel interactions to maintain the sticky gel-surface interface. First, we examined the effect of SBAA contents on the interfacial toughness of poly(HEAA-*co*-SBAA)/PEDOT: PSS hydrogels on non-porous glass substrate using the 90º peeling test. Figure 3a showed the force/width-displacement curves of poly(HEAA-*co*-SBAA)/PEDOT: PSS gels,

while Figure S8 summarized the interfacial toughness derived from force/width-displacement curves. It can be seen that without any surface modification, a small addition of SBAA (0~0.2 g) did not significantly change the network polymerization efficiency and the physical network structure, thus interfacial toughness obtained from the relatively steady plateau was 500~750 $J \cdot cm^{-2}$ and almost similar to each other. As the SBAA contents increased to 0.4~0.6 g, interfacial toughness also significantly increased to 1700~2000 $J \cdot cm^{-2}$. Further increase of SBAA contents to 0.8 g led to a slight decrease of interfacial toughness to ~1500 $J \cdot cm^{-2}$. Interfacial toughness results are consistent with bulk toughness results, indicating that both bulk toughness and strong gel-surface bindings contributes to the overall interfacial toughness.

To examine whether poly(HEAA-*co*-SBAA)/PEDOT:PSS hydrogels possessing a general surface adhesion property on different solid substrates, Figure 3b showed the debonding force-displacement curves of poly(HEAA-*co*-SBAA)/PEDOT: PSS hydrogels on the three biomedical nonporous solid surfaces (titanium, ceramic, and aluminum) and beef tissue without any pre-modification at a peeling rate of 50 $mm \cdot min^{-1}$. In our cases, the adhesion of poly(HEAA-co-SBAA)/PEDOT:PSS hydrogels to glass, aluminum, and titanium substrates was too strong to be peeled off from these substrates, i.e., the gels were broken in their bulk phase before peeling off so that no steady-state region of peeling force was presented. Thus, we used the maximal peeling force for best estimating the interfacial toughness of poly(HEAA-*co*-SBAA)/PEDOT:PSS hydrogels on different substrates. Interface toughness of the gel was ~1118 $J \cdot cm^{-2}$ on ceramic, ~1750 $J \cdot cm^{-2}$ on glass, ~1700 $J \cdot cm^{-2}$ on aluminum, ~1870 $J \cdot cm^{-2}$ on titanium, and ~1820 $J \cdot cm^{-2}$ on titanium on beef tissue, respectively (Figure S9). We also provide two videos to illustrate the typical peeling process of poly(HEAA-*co*-SBAA)/PEDOT:PSS hydrogels on beef tissue (Movie S1) and titanium (Movie S2). Visual inspection in Figure 3c confirmed that the hydrogel can be completely peeled from the ceramic surface due to the relatively smaller interfacial toughness of ~1118 $J \cdot cm^{-2}$, but on the other surfaces, strong adhesion of poly(HEAA-*co*-SBAA)/PEDOT: PSS hydrogel prevented the gels from peeling off from the surface, i.e. the gels were fractured in bulk phase before peeling off. After peeling off, some hydrogel residues were still remained on glass, aluminum, titanium, and beef tissue substrates (Figure S10).

Different interfacial toughness of the same poly(HEAA-*co*-SBAA)/PEDOT:PSS hydrogel on different substrates mainly stems from the hydrogel-substrate interaction, which in turn depends on the surface chemistry and physical lattice structure of the underlying substrates. Specially, aluminum and titanium surfaces have well-packed face-centered cubic (fcc) and hexagonal close-packed (hcp) structures, ceramic surfaces are inorganic, non-metallic and often have crystalline structures of oxide, nitride or carbide materials, and glass surfaces have non-crystalline, amorphous structures of dominant SiO_2. But, it still remains an open question about whether atomic structure and composition of a substrate affect the bonding and interactions between hydrogels and substrates. Our poly(HEAA-*co*-SBAA)/PEDOT: PSS hydrogels appear to be different from four general adhesive hydrogels as previously reported (common/tough hydrogels physically attached on solids and common/tough hydrogels chemically anchored on solids) [44] in terms of the higher adhesion strength on nonporous substrates than intrinsic mechanical strength of hydrogel matrix.

In Figure 3d, we summarized and compared the interfacial toughness of different soft materials-solid surface bonding as a function of water contents. For most of soft-adhesive materials used for biomedical applications, e.g. elastomers, tissue adhesives, and DOPA-modified or nanoparticles hydrogels, their interfacial toughness are too weak to be used for sutures and other surgical operations [45]. Differently, the other soft materials including PHEMA superglue [46] and agar/PHEAA double-network hydrogel [47] have high interfacial toughness, but low water contents, which may in turn absorb water from tissues/organisms after implantation, thus imposing the adverse healing effect. Our hydrogel with a proper balance between interfacial toughness (750-2000 $J \cdot cm^{-2}$) and water content (50~65%) is more ideal for bio-applications.

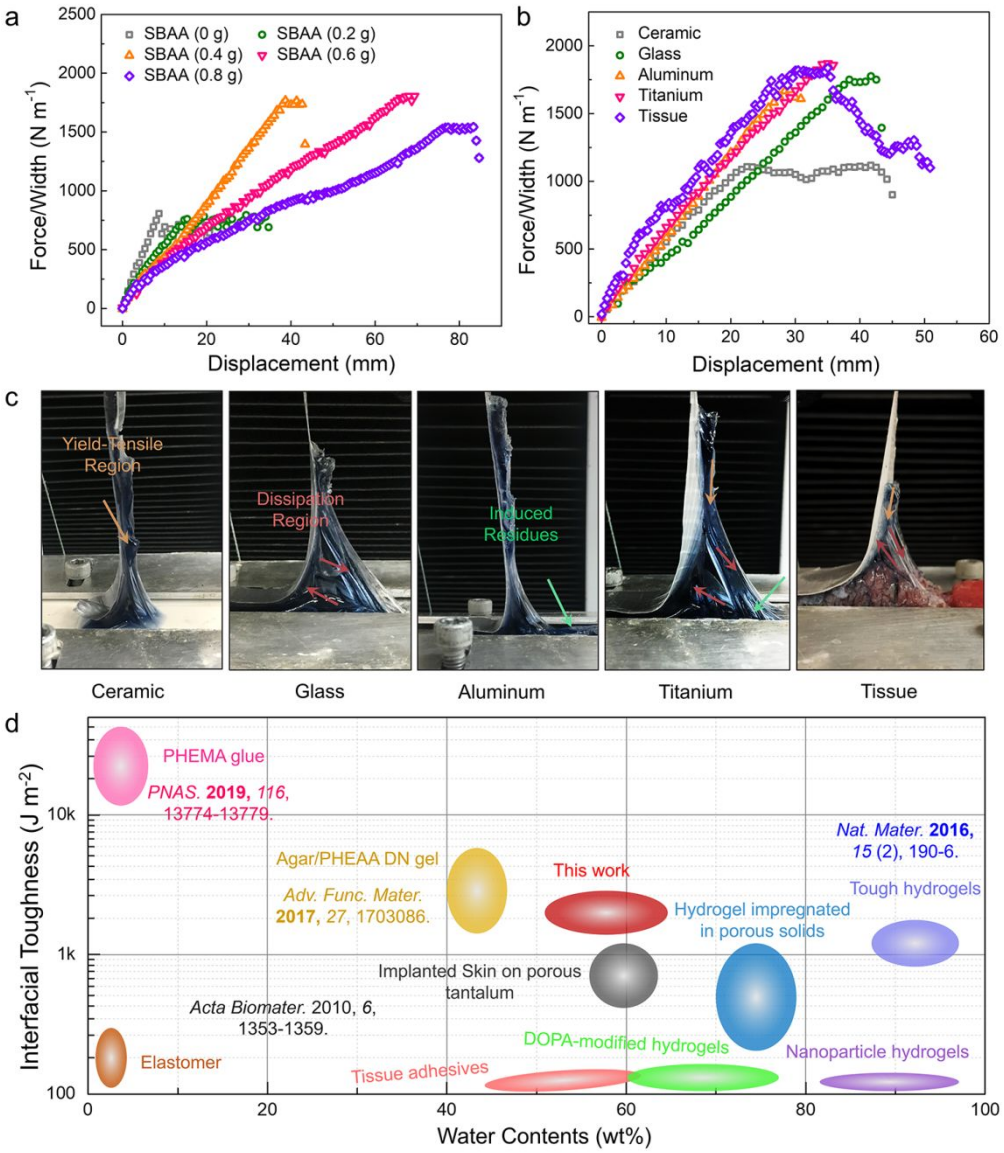

Figure 3. Interfacial toughness of poly(HEAA-*co*-SBAA)/PEDOT:PSS on different nonporous solid surfaces. (a) Peeling force/width curves of poly(HEAA-*co*-SBAA)/PEDOT: PSS hydrogels prepared with different SBAA contents (0~0.8 g) on nonporous glass at a peeling rate of 50 mm/min. (b) Peeling force/width curves of poly(HEAA-*co*-SBAA)/PEDOT:PSS hydrogels on four nonporous solid surfaces at a peeling rate of 50 mm/min. (c) Visualization of peeling off poly(HEAA-*co*-SBAA)/PEDOT: PSS hydrogels from ceramic, glass, titanium, aluminum, and beef tissue surfaces. (d) A summary and comparison of different conductive and adhesive materials on non-porous solids for their interfacial toughness vs. water contents (wt%).

Strain-induced conductivity and sensitivity of poly(HEAA-*co*-SBAA)/PEDOT: PSS hydrogels

In this subsection, we aimed to demonstrate that poly(HEAA-*co*-SBAA)/PEDOT: PSS hydrogel can be used as a self-adhesive/stretching- and pressure-sensitive strain sensor for detecting different human movements (finger gestures, knee bending, and speaking) (Figure 4a). First, we characterized the electrochemical kinetics and ionic resistance by electrochemical impedance spectroscopy (EIS). Figure 4b showed that at the low frequency region, the slope of the EIS plot was close to ~60°, indicating a good capacitive behavior, but at the high frequency region, a relatively small series resistance of ~160 $\Omega \cdot m^{-1}$ were observed, reflecting a very small charge transfer resistance in electrode system. High charge-transfer kinetics is possibly attributed to the charge-rich sites and conjugated structures of the conductive polymers inside the polyzwitterionic networks.

Upon demonstrating high charge-transfer kinetics of poly(HEAA-*co*-SBAA)/PEDOT: PSS hydrogels, we examined the strain-induced electromechanical sensitivity of bulk poly(HEAA-*co*-SBAA)/PEDOT: PSS hydrogels, as measured by the relative resistance change $\frac{\Delta R}{R_0} = \frac{R_r - R_0}{R_0}$, where R_r was the real-time resistance and R_0 was the original resistance without any external loading. Figure 4c showed that when poly(HEAA-*co*-SBAA)/PEDOT: PSS hydrogels were stretched to 150%, 300%, 500%, and 900% at different stretching rates, the hydrogels exhibited obvious strain-induced responses, as evidenced by a large increase in the relative resistance change as strains from ~16%, ~150%, ~500%, to ~1550%. The sensitivity of the hydrogel at a 900% strain was 18-times higher than that of the hydrogel at a 150% strain. Moreover, the stretching sensing performances at large tensile strain of 1000% and 1200% were provided in Figure S11, which showed a distinct shifting of relative resistance baselines after several loading-unloading cycles. This again indicates that the internal network deformation cannot be fully and immediately recovered, leading to the baseline shifting. In parallel to stretching, we also applied the pressure to compress the hydrogel to 1/2, 1/3, and 1/4 of the original strain, the relative resistance was reduced to ~92%, ~80%, and ~72% relative to the control, respectively (Figure 4d). In both cases, the electromechanical loading-unloading curves were stable over 10 cycles without any signal decay at different-scale stretching and compression, indicating a robust sensing reproducibility.

Due to high strain-induced bulk sensitivity of poly(HEAA-*co*-SBAA)/PEDOT: PSS hydrogels, we further examined the strain-induced sensitivity at the hydrogel-surface interface to monitor different human motions (i.e. the first author's finger, hand, knee, and throat). Due to excellent surface adhesiveness and structural flexibility,

poly(HEAA-*co*-SBAA)/PEDOT: PSS hydrogels can conformably and tightly adhere onto different epidermis of human body without using any additional glue or tapes. After adhering poly(HEAA-*co*-SBAA)/PEDOT: PSS hydrogels to the index finger and knee separately (Figure 4e and 4f), the bending of the index finger and knee to 90^{o} resulted in an immediate increase of the relative resistance to ~3.2% and ~4.5%, respectively. Remaining the bending status did not induce any change in relative resistances, indicating a good electrical signal stability. After straightening them back to the original status, both relative resistances rapidly returned to the baseline. Moreover, we attached the hydrogel to the first author's throat for detecting the possible vibrations of vocal cords. Figure 4g showed that when speaking a "UAKRON," [yoo 'ækrən] word, four distinct peaks were observed and correlated with four pronunciation bytes of U [yoo], A [æ], K [k], Ron [rən]. Speaking the "UAKRON" word multiple times led to almost identical response signals (i.e., relative resistance change), indicating stable sensing repeatability. Apart from stretching-induced interfacial sensitivity, we further tested the pressure-induced interfacial sensitivity by fabricating a sandwich-like hydrogel sensor made of poly(HEAA-*co*-SBAA)/PEDOT: PSS hydrogel in between two copper backings. The resultant sensor can accurately detect the upward stepwise changes of relative resistance as the pressure reduced from 1000 N to 100 N, followed by the almost same downward ladder as the pressure increased (Figure 4h). Additionally, in a pressure range of 100~400 N, the change of relative resistance seemed to follow a linear relationship, but as pressure further increased, the nonlinear relationship occurred, indicating that the pressure-induced sensibility could be derived from the transient relaxation of internetwork changes. More importantly, much weaker pressure-sensitive signals could be detected. As the hydrogel sensor attached on the Author wrists, steady and repeatable pulses of ~68 beats per min can be detected at the relax condition, but after exercise pulse was increased to ~84 beats per min (Figure 4i). Figure 4j further demonstrated that poly(HEAA-*co*-SBAA)/PEDOT:PSS hydrogel sensor enabled to well detect resistance change by continuous dripping water droplets of ~50 μL, falling from a height of 10 cm onto sensor matrix. Overall, poly(HEAA-*co*-SBAA)/PEDOT: PSS hydrogels demonstrate their high sensitivity, stability, and repeatability to monitor and distinguish the strain-induced signals in bulk and at interface in a fast response time of <0.025 s.

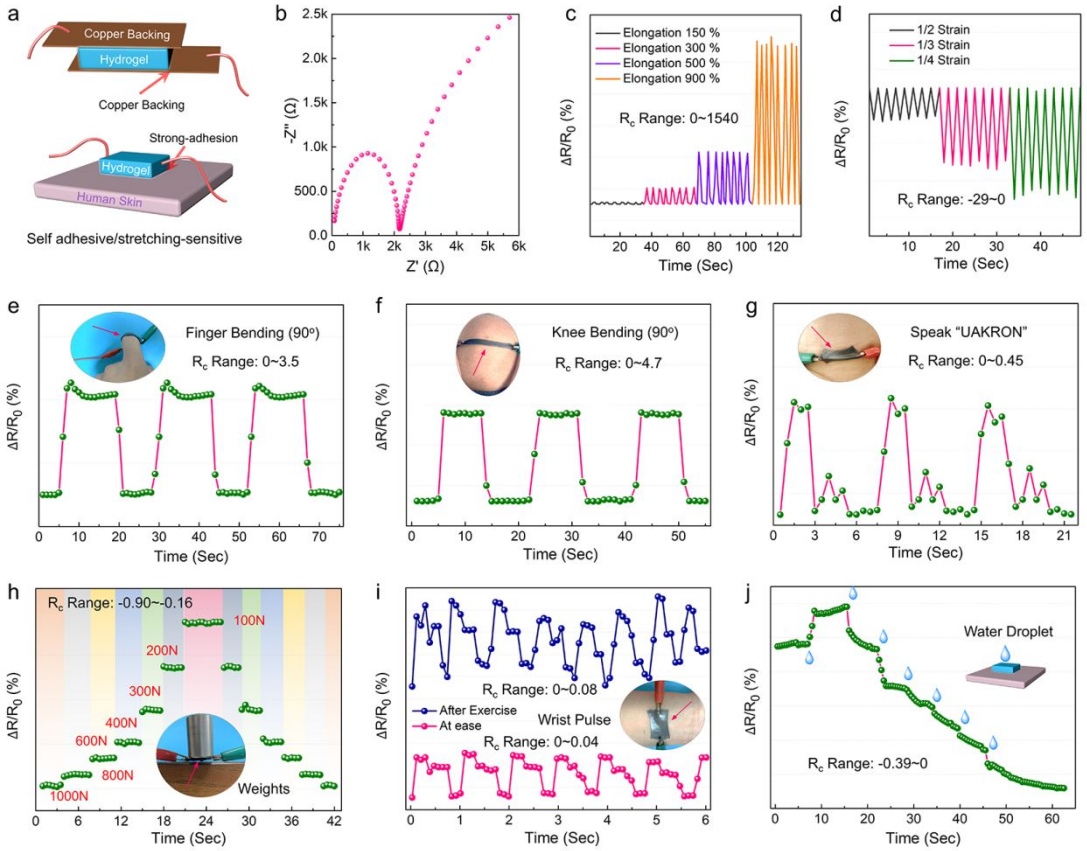

Figure 4. Electrochemical sensitivity of poly(HEAA-*co*-SBAA)/PEDOT:PSS hydrogel strain sensor in bulk hydrogel and at human-hydrogel interface. (a) Schematic illustration of stretching-induce and pressure-induced interfacial hydrogel strain sensors. (b) Electrochemical impedance spectroscope of poly(HEAA-*co*-SBAA)/PEDOT: PSS hydrogel in a frequency range of 0.01-1 MHz. Relative resistance changes of bulk hydrogel sensors in response to repeatable (c) stretching/release and (d) compression/release motions at different strains. Relative resistance changes of interfacial hydrogel sensors in response to repeatable (e) finger bending, (f) knee bending, and (g) vocal word of "UAkron". (h) Pressure-dependent interfacial hydrogel strain sensors in response to pressure changes from 100 N to 1000 N, (i) wrist pulse before and after exercise, and (j) continuous water droplet.

Almost all of hydrogel-based strain sensors as reported in literature were tested for their strain-induced sensing performance and mechanical properties separately, thus there is a lack of rigorous relationship between network structure change (i.e. as reflected by mechanical properties) and sensing performance. To bridge this gap, we constructed a new mechanosensing platform by connecting a universal tensile machine and an electrochemical workstation, which can truly realize the real-time monitoring of electrical signals and mechanical properties in response to strains (Figure 5a). Briefly, as dumb-bell shape hydrogels are stretched to different strains at a certain rate, both tensile stress and relative resistance will be simultaneously recorded for comparison, as reflected by strain-induced network structure changes in a real time. Figure 5b and Figure S12 showed the tensile stress and current curves in response to the stretching of poly(HEAA-*co*-SBAA)/PEDOT:PSS hydrogel at a slow rate of 20 mm/min. It is interesting to observe that at a small strain of 300% right after a yielding point, a significant increase in current, in concurrence with an increase of tensile stress. Before

and after this strain, the changes of current and tensile stress showed opposite trends, i.e., current decreased while tensile stress increased. Such rapid current increase from ~0.08 mA to ~0.14 mA indicates a dramatic drop of relative resistance. Such phenomena in both Figure 5b and Figure S12 was only observed at a lower stretching rate of ~20 mm/min. A low stretching rate allows to gradually engage short-range ionic interactions between zwitterionic networks, optimizes conductive pathways for charge transfer, and thus causes a temporary decrease of relative resistance at an early and small stretching stage. We did not observe this phenomenon at a stretching rate of ≥40 mm/min, indicating that short-range ionic interactions are time and spatial dependent. Therefore, this singular sensing curve makes our poly(HEAA-*co*-SBAA)/PEDOT: PSS hydrogel different from other hydrogel-based strain sensors (Figure 5c). In parallel to experiments, we also performed a Moldflow simulation to map out the stress distribution of poly(HEAA-*co*-SBAA)/PEDOT: PSS hydrogel at a strain of 2000% (Figure 5d). Simulation showed that the maximum tensile stress of the hydrogel was ~0.30 MPa (close to experimental value of ~0.34 MPa) and located in the center of the hydrogel, and tensile stress gradually decayed as a separation distance from the center region.

Figure 5e and Table S2 summarized gauge factor and tensile strain of our hydrogel strain sensor with other fully polymer-based strain sensors. We excluded nanocomposite hydrogel strain sensors containing carbon-based nanomaterials, noble metal-based nanomaterials, or ion liquids from comparison [16, 20-22, 33, 34, 48-52]. Among these conductive polymer hydrogel sensors and salt-incorporated polymer sensors, including PIL-BF_4/PEDGA, LiCl-polyAAm, NaCl-polyAAm, NaCl-gelatin/PVA, PVA/RSF/borax, and PDA/polyAAm, have comparable gauge factor of ~1.0 with varied strains of 500%-5000%, while only two hydrogel sensors of PANI-poly(AAm-*co*-HEMA) and polyNIPAAm/PANI have large gauge factor of 11 and 3.9 but relatively small strains of 200-300%. Using a 1000% strain as cutoff value, only six hydrogel sensors possess ultra-strechability, and among them, our poly(HEAA-*co*-SBAA)/PEDOT: PSS hydrogel outperforms others in terms of both gauge factor of ~2.0 and stretchability of ~5000%, not even mention other superior mechanical properties including bulk and interfacial toughness, self-recovery, and self-healing. Since our poly(HEAA-*co*-SBAA)/PEDOT:PSS hydrogel used PEDOT:PSS as conducting additives, its amount was quite low (~0.20 wt% of solid content), while other reported full-polymer hydrogels contain a high amount of conductive polymers (0.6~5.0 wt%) and used them as polymer network. For comparison, on one hand, poly(HEAA-*co*-SBAA)/PEDOT:PSS hydrogel (2-2.5) has the lower gauge factor than the abovementioned full-polymer hydrogels (2.0~10.0). On the other hand, our hydrogel sensors outperformed these polymer strain sensors in terms of mechanical properties, which suffered from weak mechanical strength of 10-200 kPa, low stretchability of <1000%, and poor fatigue resistance to sustain multiple times of loading-unloading cycles. Apart from full polymer hydrogel sensors, carbon-based or noble metal-based strain sensors have a large gauge factor of 2.0~100, but they only tolerate small stretchability (1%~300%). Elastomer-based strain sensors incorporated with conductive composites are more stretchable, but biocompatibility is a big issue.

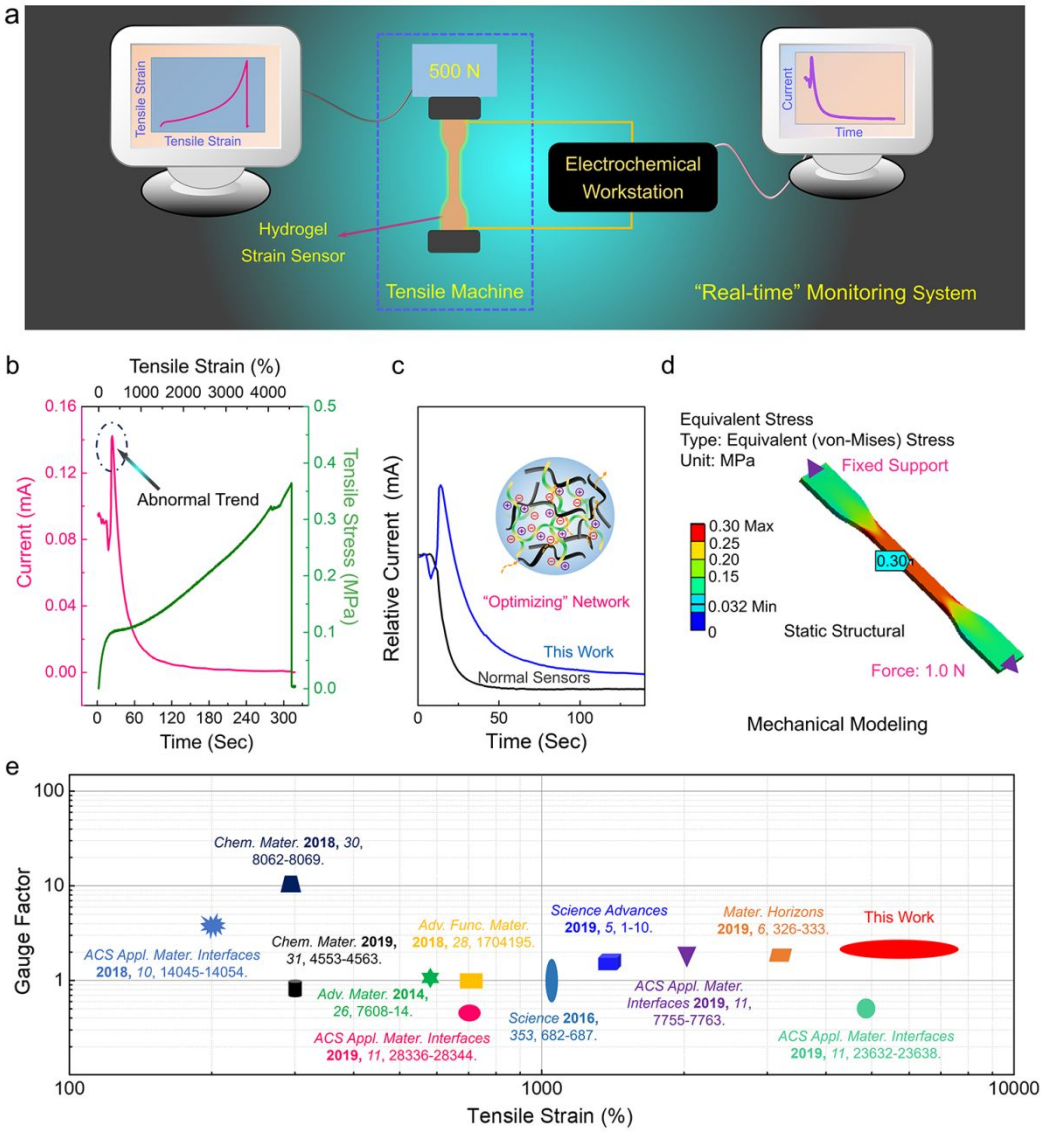

Figure 5. (a) Schematic illustration of an in-house mechanosensing platform by connecting a universal tensile machine and an electrochemical workstation to real-time and simultaneously measure strain-induced tensile stress and currency. (b) Strain-induced tensile stress and current sensing curves of poly(HEAA-*co*-SBAA)/PEDOT:PSS hydrogel sensor. (c) Comparison of time-dependent relative current changes between poly(HEAA-*co*-SBAA)/PEDOT:PSS hydrogel sensor and a representative polymer-based hydrogel strain sensors. (d) Moldflow simulation of conductive hydrogel to show stress distribution. (e) Comparison of gauge factor and tensile strain between poly(HEAA-*co*-SBAA)/PEDOT: PSS sensor and other polymeric hydrogel-based strain sensors. [16, 20-22, 33, 34, 48-52]

Antifouling and biocompatibility of poly(HEAA-*co*-SBAA)/PEDOT: PSS hydrogels

Many wearable sensing devices are devoted to improving their sensing ability, but somehow ignore their biocompatibility[18, 53, 54]. Here, we further investigated the antifouling property of poly(HEAA-*co*-SBAA)/PEDOT: PSS hydrogel using both bacteria and cell assays. A well-known antifouling polyHEAA hydrogel and pure polystyrene flask were selected as positive and negative controls for comparison.

PolyHEAA hydrogels alone exhibited strong surface resistance to both *E. coli* and *S. aureus* attachment, as evidenced by adhered density of ~2.35×10^4 and ~1.58×10^4 cells·cm^{-2} after 12 h culture, respectively (Figure 6a), consistent with our previous studies [55, 56]. Interestingly, poly(HEAA-*co*-SBAA)/PEDOT: PSS hydrogels showed even better bacterial resistance, i.e. ~1.57×10^4 cells·cm^{-2} of *S. epider.* and ~0.52×10^4 cells·cm^{-2} of *E. coli* on the hydrogel surface showed a decrease of 33% and 67% of bacterial adhesion as compared to polyHEAA hydrogels (Figure 6b). Note that both polyHEAA and poly(HEAA-*co*-SBAA)/PEDOT:PSS hydrogels was still considered as antifouling materials, as compared to the almost full surface coverage of bacteria and BAECs on the surface of polystyrene flask (Figure 6c). These results are mainly attributed to the enhanced antifouling property from zwitterionic polySBAA [55-57]. On the basis of the excellent resistance of poly(HEAA-*co*-SBAA)/PEDOT: PSS hydrogel against bacterial adhesion, we further challenged poly(HEAA-*co*-SBAA)/PEDOT: PSS and polyHEAA hydrogels with bovine aortic endothelial cell (BAECs). Consistently, after 72 h co-culture of hydrogels with BAECs at 37 °C, poly(HEAA-*co*-SBAA)/PEDOT:PSS hydrogel adsorbed ~0.15×10^4 cells·cm^{-2} of BAECs, which was lower than ~0.34×10^4 cells·cm^{-2} of adhered BAECs on polyHEAA hydrogel (Figure 6d).

Cytotoxicity is another critical factor for applying sensing devices to bio-applications. Figure 6e showed the side-by-side comparison of cell viability of poly(HEAA-*co*-SBAA)/PEDOT: PSS and polyHEAA hydrogels using MTT assay with SH-SY5Y cell line. The relative cell viability (%) of any hydrogel is normalized by the untreated cells. As a control, polyHEAA gel presented almost no cytotoxicity to cells, as evidenced by ~97.6% cell viability during 24 h culture, and further increase cell culture time to 48 h only slightly reduced the cell viability by ~3%. Consider that cell apoptosis is inevitable during cell culture, thus such slight decrease of cell viability could account for negligible. Similarly, poly(HEAA-*co*-SBAA)/PEDOT: PSS hydrogels also exhibited relatively low cytotoxicity, where cell viability was 95.0% at 24 h and ~91.2% at 48 h. Meanwhile, we also used the LDH assay to re-examine cell cytotoxicity of these two hydrogels and the results were summarized in Figure S13. As expected, polyHEAA hydrogel only induced very low cell toxicity of 4% at 24 h and 8% at 48 h, demonstrating good biocompability and consistent with MTT results. Poly(HEAA-*co*-SBAA)/PEDOT: PSS hydrogels induced 8% and 10% cell death at 24 h and 48 h, showing a slightly higher but still tolerable cytotoxicity than polyHEAA hydrogels. This could be due to our observation that the acid environment as provided by interpenetrated conductive PEDOT: PSS polymers partially inhibited the growth of SH-SY5Y cells.

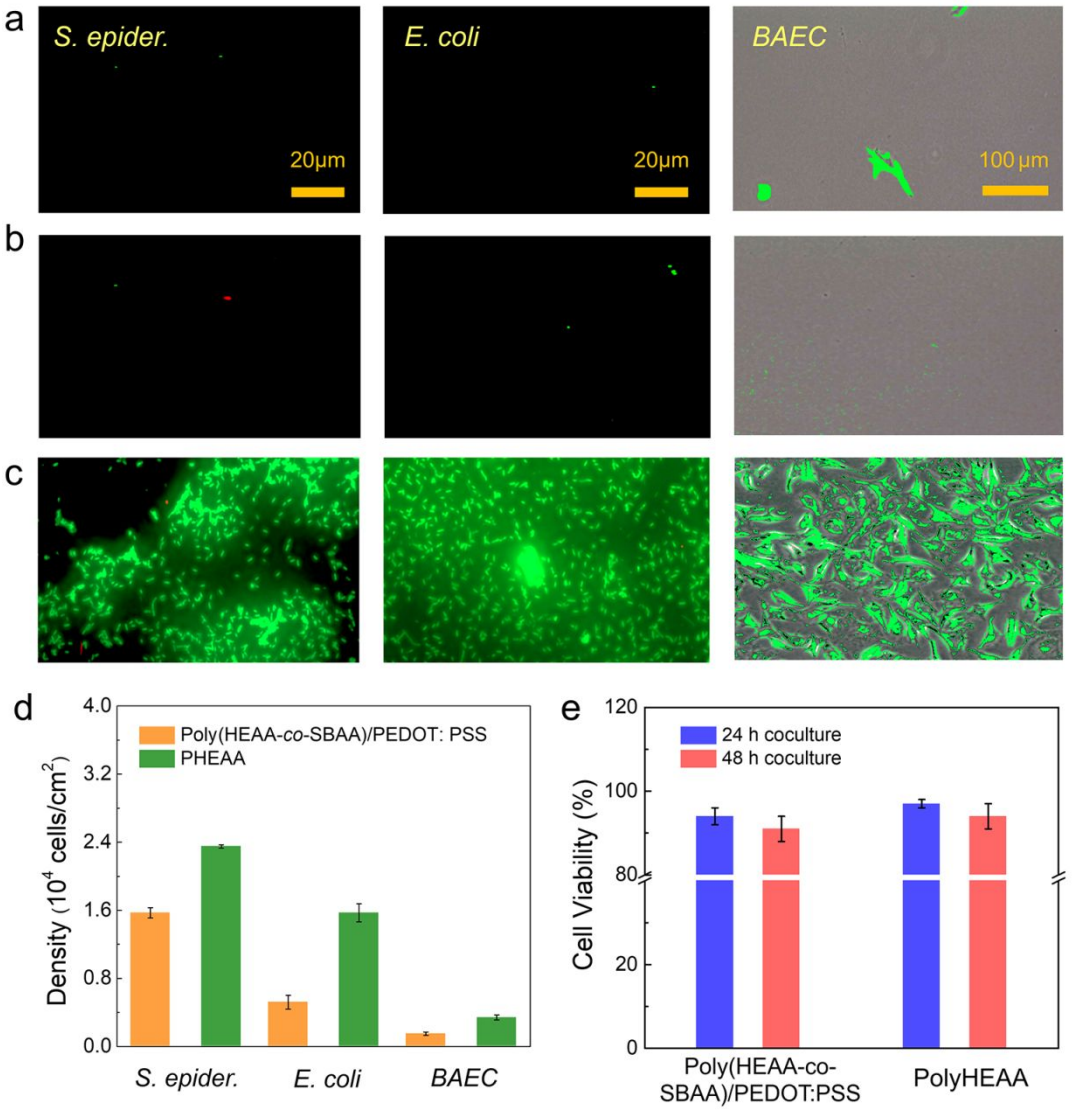

Figure 6. Antifouling and biocompatibility of poly(HEAA-*co*-SBAA)/PEDOT:PSS hydrogel. Representative fluorescence microscopy images to show the attachment of *S. epidermidis* (left), *E. coli* (center), and *BAEC* (right) on (a) polyHEAA hydrogel, (b) poly(HEAA-*co*-SBAA)/PEDOT: PSS hydrogel, and (c) pristine polystyrene flask at 37 °C for 12 h culture with bacteria or 72 h culture with cells. (d) Statistics analysis of bacterial and cell density on polyHEAA and poly(HEAA-*co*-SBAA)/PEDOT: PSS hydrogels, derived from (a) and (b). (e) MTT assay to show cell viability with polyHEAA and poly(HEAA-*co*-SBAA)/PEDOT: PSS hydrogels after 24 h and 48 h incubation of SH-SY5Y cell line.

Conclusions

In this work, we designed and fabricated a fully polymeric conductive and tough hydrogel, consisting of interpenetrating networks of conductive PEDOT: PSS polymers and zwitterionic poly(HEAA-*co*-SBAA) polymers. The resultant poly(HEAA-*co*-SBAA)/PEDOT: PSS hydrogels achieved a combination of superior mechanical, conductive, and biocompatible properties, which enabled the hydrogels to be served as self-adhesive/stretching- and pressure-sensitive strain sensor for detecting different human movements (finger gestures, knee bending, and speaking). Specifically, due to the IPN network, reversible hydrogen bonds within HEAA and SBAA, and electrostatic

interactions between PEDOT: PSS and SBAA, poly(HEAA-*co*-SBAA)/PEDOT: PSS hydrogels achieved ultra-high stretchability of 4000-5000%, tensile stress of ~0.5 MPa, rapid toughness/stiffness recovery of 70%/80% within 5 min, and fast self-healing (<3 min). The hydrogel also exhibited a general and strong surface adhesion of ~1700 $J \cdot cm^{-2}$ on different nonporous solid surfaces (e.g., glass, titanium, ceramic, aluminum, and beef tissue). Secondly, the hydrogels showed high sensitivity (gauge factor= 2.0) and high conductivity of 0.625 S/m at low strain and outstanding nonlinearity at high strains, which are attributed to synergistic electrostatic interactions between high charge-density zwitterionic polySBAA and conductive PEDOT: PSS chains. Thirdly, a combination of superior mechanical, self-adhesive, and conductive properties endowed the hydrogels to be further designed into dual-sensitive strain sensors, enabling to real-time detect subtle human motions (finger bending, knee bending, and vocal voice). Finally, poly(HEAA-*co*-SBAA)/PEDOT:PSS hydrogels also exhibited excellent antifouling properties to resist bacterial and cell adhesion. In addition, an in-house mechanosensing platform was designed to realize the real-time monitoring of strain-induced tensile stress and electronic resistance simultaneously, which allowed to better establish the structure-sensing relationship of hydrogels. This work provides a new fully polymeric hydrogel system with high sensitivity, high mechanical stability, and biocompatibility, which acts as strain sensor for human-machine interaction and healthcare monitoring beyond those nanocomposite-based or elastomer-based strain sensors.

Acknowledgment. J. Z. thanks financial supports from NSF (CMMI-1825122 and DMR-1806138).

References

1. C. M. Boutry, Y. Kaizawa, B. C. Schroeder, A. Chortos, A. Legrand, Z. Wang, J. Chang, P. Fox and Z. Bao, *Nat. Electronics*, 2018, **1**, 314-321.
2. S. Choi, H. Lee, R. Ghaffari, T. Hyeon and D. H. Kim, *Adv. Mater.*, 2016, **28**, 4203-4218.
3. L. Li, Y. Wang, L. Pan, Y. Shi, W. Cheng, Y. Shi and G. Yu, *Nano Lett.*, 2015, **15**, 1146-1151.
4. A. Chortos, J. Liu and Z. Bao, *Nat. Mater.*, 2016, **15**, 937-950.
5. C. Yang and Z. Suo, *Nat. Rev. Mater.*, 2018, **3**, 125-142.
6. Y. Xu, Z. Lin, X. Huang, Y. Wang, Y. Huang and X. Duan, *Adv. Mater.*, 2013, **25**, 5779-5784.
7. X. Liu, C. Steiger, S. Lin, G. A. Parada, J. Liu, H. F. Chan, H. Yuk, N. V. Phan, J. Collins, S. Tamang, G. Traverso and X. Zhao, *Nat. Commun.*, 2019, **10**, 493.
8. B. Lu, H. Yuk, S. Lin, N. Jian, K. Qu, J. Xu and X. Zhao, *Nat. Commun.*, 2019, **10**, 1043.
9. S. Mao, D. Zhang, Y. Zhang, J. Yang and J. Zheng, *Advanced Functional Materials*, 2020, DOI: 10.1002/adfm.202004633, 2004633.
10. D. Zhang, B. Ren, Y. Zhang, L. Xu, Q. Huang, Y. He, X. Li, J. Wu, J. Yang, Q. Chen, Y. Chang and J. Zheng, *J Mater Chem B*, 2020, **8**, 3171-3191.
11. D. Zhang, F. Yang, J. He, L. Xu, T. Wang, Z.-Q. Feng, Y. Chang, X. Gong, G. Zhang and J. Zheng, *ACS Applied Polymer Materials*, 2019, **2**, 1031-1042.
12. T. Yamada, Y. Hayamizu, Y. Yamamoto, Y. Yomogida, A. Izadi-Najafabadi, D. N. Futaba and K. Hata, *Nat. Nanotechnol.*, 2011, **6**, 296-301.
13. R. Nur, N. Matsuhisa, Z. Jiang, M. O. G. Nayeem, T. Yokota and T. Someya, *Nano Lett.*, 2018, **18**, 5610-5617.
14. Z. Lei, Q. Wang, S. Sun, W. Zhu and P. Wu, *Adv. Mater.*, 2017, **29**, 1700321
15. Z. Lei and P. Wu, *ACS Nano*, 2018, **12**, 12860-12868.
16. Y. Ren, J. Guo, Z. Liu, Z. Sun, Y. Wu, L. Liu and F. Yan, *Sci. Adv.*, 2019, **5**, 1-10.
17. Yi-Zhou Zhang, Kang Hyuck Lee, Dalaver H. Anjum, Rachid Sougrat, Qiu Jiang, Hyunho Kim and H. N. Alshareef, *Sci. Adv.*, 2018, **4**.
18. G. Cai, J. Wang, K. Qian, J. Chen, S. Li and P. S. Lee, *Adv. Sci.*, 2017, **4**, 1600190.
19. H. Gu, H. Zhang, C. Ma, H. Sun, C. Liu, K. Dai, J. Zhang, R. Wei, T. Ding and Z. Guo, *J. Mater. Chem. C*, 2019, **7**, 2353-2360.
20. Chong-Chan Kim, Hyun-Hee Lee, Kyu Hwan Oh and J.-Y. Sun, *Science*, 2016, **353**, 682-687.
21. J. Y. Sun, C. Keplinger, G. M. Whitesides and Z. Suo, *Adv. Mater.*, 2014, **26**, 7608-7614.
22. Z. Wang, J. Chen, Y. Cong, H. Zhang, T. Xu, L. Nie and J. Fu, *Chem. Mater.*, 2018, **30**, 8062-8069.
23. S. Ryu, P. Lee, J. B. Chou, R. Z. Xu, R. Zhao, A. J. Hart and S. G. Kim, *ACS Nano*, 2015, **9**, 5929-5936.
24. S. A. Chowdhury, M. C. Saha, S. Patterson, T. Robison and Y. Liu, *Adv. Mater. Technol.*, 2019, **4**, 1800398.
25. R. Y. Tay, H. Li, J. Lin, H. Wang, J. S. K. Lim, S. Chen, W. L. Leong, S. H. Tsang and E. H. T. Teo, *Adv. Func. Mater.*, 2020, **30**, 1909604.
26. Q. J. Sun, X. H. Zhao, Y. Zhou, C. C. Yeung, W. Wu, S. Venkatesh, Z. X. Xu, J. J. Wylie, W. J. Li and V. A. L. Roy, *Adv. Func. Mater.*, 2019, **29**, 1808829.

27. J. C. Yeo, H. K. Yap, W. Xi, Z. Wang, C.-H. Yeow and C. T. Lim, *Adv. Mater. Technol.*, 2016, **1**, 1600018.
28. S. Cheng and Z. Wu, *Adv. Func. Mater.*, 2011, **21**, 2282-2290.
29. P. Li, Z. Jin, L. Peng, F. Zhao, D. Xiao, Y. Jin and G. Yu, *Adv. Mater.*, 2018, **30**, e1800124.
30. K. Xu, H. Sun, T. P. Ruoko, G. Wang, R. Kroon, N. B. Kolhe, Y. Puttisong, X. Liu, D. Fazzi, K. Shibata, C. Y. Yang, N. Sun, G. Persson, A. B. Yankovich, E. Olsson, H. Yoshida, W. M. Chen, M. Fahlman, M. Kemerink, S. A. Jenekhe, C. Muller, M. Berggren and S. Fabiano, *Nat. Mater.*, 2020, DOI: 10.1038/s41563-020-0618-7, 1-7.
31. H. Numazawa, K. Sato, H. Imai and Y. Oaki, *NPG Asia Mater.*, 2018, **10**, 397-405.
32. H. Yuk, B. Lu, S. Lin, K. Qu, J. Xu, J. Luo and X. Zhao, *Nat Commun*, 2020, **11**, 1604.
33. J. Chen, Q. Peng, T. Thundat and H. Zeng, *Chem. Mater.*, 2019, **31**, 4553-4563.
34. Z. Wang, H. Zhou, W. Chen, Q. Li, B. Yan, X. Jin, A. Ma, H. Liu and W. Zhao, *ACS Appl. Mater. Interfaces*, 2018, **10**, 14045-14054.
35. J. Park, S. Wang, M. Li, C. Ahn, J. K. Hyun, D. S. Kim, D. K. Kim, J. A. Rogers, Y. Huang and S. Jeon, *Nat. Commun.*, 2012, **3**, 916.
36. M. A. Darabi, A. Khosrozadeh, R. Mbeleck, Y. Liu, Q. Chang, J. Jiang, J. Cai, Q. Wang, G. Luo and M. Xing, *Adv. Mater.*, 2017, **29**, 1700533.
37. Y. Zhu, N. Li, T. Lv, Y. Yao, H. Peng, J. Shi, S. Cao and T. Chen, *J. Mater. Chem. A*, 2018, **6**, 941-947.
38. Y. Y. Lee, H. Y. Kang, S. H. Gwon, G. M. Choi, S. M. Lim, J. Y. Sun and Y. C. Joo, *Adv. Mater.*, 2016, **28**, 1636-1643.
39. M. R. Moraes, A. C. Alves, F. Toptan, M. S. Martins, E. M. F. Vieira, A. J. Paleo, A. P. Souto, W. L. F. Santos, M. F. Esteves and A. Zille, *J. Mater. Chem. C*, 2017, **5**, 3807-3822.
40. S. Lim, C. Y. Yap, Y. L. Pang and K. H. Wong, *J. Hazard. Mater.*, 2020, **390**, 121532.
41. M. Xiao, E. Gonzalez, A. M. Monterroza and M. Frey, *Carbohydr. Polym.*, 2017, **174**, 626-632.
42. Q. Chen, H. Chen, L. Zhu and J. Zheng, *J. Mater. Chem. B*, 2015, **3**, 3654-3676.
43. X. Zhao, *Soft Matter*, 2014, **10**, 672-687.
44. H. Yuk, T. Zhang, S. Lin, G. A. Parada and X. Zhao, *Nat. Mater.*, 2016, **15**, 190-196.
45. T. Kurokawa, H. Furukawa, W. Wang, Y. Tanaka and J. P. Gong, *Acta Biomater*, 2010, **6**, 1353-1359.
46. Hyesung Cho, Gaoxiang Wu, Jason Christopher Jolly, Nicole Fortoul, Zhenping He, Yuchong Gao, Anand Jagota and S. Yang, *Proc. Natl. Acad. Sci. U. S. A.*, 2019, **116**, 13774-13779.
47. H. Chen, Y. Liu, B. Ren, Y. Zhang, J. Ma, L. Xu, Q. Chen and J. Zheng, *Adv. Func. Mater.*, 2017, **27**, 1703086.
48. H. Chen, X. Ren and G. Gao, *ACS Appl. Mater. Interfaces*, 2019, **11**, 28336-28344.
49. X. Zhang, N. Sheng, L. Wang, Y. Tan, C. Liu, Y. Xia, Z. Nie and K. Sui, *Mater Horiz*, 2019, **6**, 326-333.
50. N. Yang, P. Qi, J. Ren, H. Yu, S. Liu, J. Li, W. Chen, D. L. Kaplan and S. Ling, *ACS Appl. Mater. Interfaces*, 2019, **11**, 23632-23638.

51. L. Han, K. Liu, M. Wang, K. Wang, L. Fang, H. Chen, J. Zhou and X. Lu, *Adv. Func. Mater.*, 2018, **28**, 1704195.
52. H. Qiao, P. Qi, X. Zhang, L. Wang, Y. Tan, Z. Luan, Y. Xia, Y. Li and K. Sui, *ACS Appl. Mater. Interfaces*, 2019, **11**, 7755-7763.
53. X. Liu, C. Tang, X. H. Du, S. A. Xiong, S. Y. Xi, Y. F. Liu, X. Shen, Q. B. Zheng, Z. Y. Wang, Y. Wu, A. Horner and J. K. Kim, *Mater Horiz*, 2017, **4**, 477-486.
54. S. Chun, Y. Choi and W. Park, *Carbon*, 2017, **116**, 753-759.
55. D. Zhang, Y. Fu, L. Huang, Y. Zhang, B. Ren, M. Zhong, J. Yang and J. Zheng, *J. Mater. Chem. B*, 2018, **6**, 950-960.
56. Y. Wang, J. Wu, D. Zhang, F. Chen, P. Fan, M. Zhong, S. Xiao, Y. Chang, X. Gong, J. Yang and J. Zheng, *J. Mater. Chem. B*, 2019, **7**, 5762-5774.
57. D. Zhang, B. Ren, Y. Zhang, Y. Liu, H. Chen, S. Xiao, Y. Chang, J. Yang and J. Zheng, *J Colloid Interface Sci*, 2020, **578**, 242-253.